Electronic Supplementary Material (ESI) for Dalton Transactions.

Supporting Information

An Unprecedented $\{Cu^{II}_{14}Te^{IV}_{10}\}$ Core Incorporated in a 36-Tungsto-4-Silicate Polyoxometalate with Visible Light-Driven Catalytic Hydrogen Evolution Activity

Wei-Chao Chen, Si-Tong Wu, Chao Qin, Xin-Long Wang, Kui-Zhan Shao, Zhong-Min Su* and En-Bo Wang*

Key Lab of Polyoxometalate Science of Ministry of Education, Institute of Functional Material Chemistry, Faculty of Chemistry, Northeast Normal University, Changchun, 130024 Jilin, People's Republic of China.

CONTENTS

Section 1 Synthesis, Crystal Data, and Structure of 1

General Considerations. $Na_{10}[A\text{-}\alpha\text{-}SiW_9O_{34}]\cdot 18H_2O$ was synthesized according to the literature method. (*Inorg. Chem.* 1977, *16*, 2115) All commercially obtained reagent, including Na_2TeO_3, $CuCl_2\cdot 2H_2O$, Na_2CO_3, and HCl were purchased from Aldrich and used without further purification. The reaction mixtures were heated and agitated in the round bottomed flasks with reflux condensing tubes on a CL-1A-type agitator purchased from GongYi Company in China. Deionized water was used throughout the study. A pHS-25B pH meter was used for pH measurements.

1.1 Synthesis

$CuCl_2\cdot 2H_2O$ (0.10 g, 0.60 mmol) and Na_2TeO_3 (0.13 g, 0.58 mmol) were added into 40 mL of distilled water separately, and then $Na_{10}[A\text{-}\alpha\text{-}SiW_9O_{34}]\cdot 18H_2O$ (1.18 g, 0.40 mmol) and Na_2CO_3 (0.05 g, 0.47 mmol) were added. The mixture was stirred for further 30 min. After that the pH was adjusted to 8.0 by 2.0 M HCl (aq). The resulting turbid solution was heated to 70 ^{o}C stirred for another 1 h, and then filtered. The filtrate was kept in a 50 mL beake sealed by film with a few of tiny pores, and very slowly evaporated at room temperature. After about five weeks, green needle-like crystals suitable for X-ray crystallography were obtained, washed with cold water, and air-dried to give 46 mg of **1** (8.30% yield base on Cu). IR (KBr disk v/cm^{-1}): 3419(w), 1607(s), 940(w), 899(s), 800(m), 753(w). Elemental anal. Calcd (%) (found): Cu 7.24 (7.18), Na 1.68 (1.87), W 53.87 (54.21).

1.2 Crystal Data

Table S1. Crystal Data and Structure Refinements for **1**.

	1
Empirical formula	$Cu_{14}H_{62}Na_9O_{195}Si_4Te_{10}W_{36}$
M	12285.92
λ/Å	0.71073
T/K	296(2)
Crystal system	Tetragonal
Space group	I-42*d*
a/Å	34.7169(13)
b/Å	34.7169(13)
c/Å	45.3651(19)
α/°	90
β/°	90
γ/°	90
V/Å^3	54677(5)
Z	8
D_c/Mg m^{-3}	2.985
μ/mm^{-1}	17.300
F(000)	42936
ϑ Range/°	1.477–25.151
Measured reflections	158630
Independent reflections	24385
R_{int} after SQUEEZE	0.0999
Goodness-of-fit on F^2	0.999
$R_1(I > 2\sigma(I))^a$	0.0555
wR_2 (all data)^b	0.1521

$^aR_1 = \sum||F_o| - |F_c||/\sum|F_o|$. $^bwR_2 = \{\sum[w(F_o^2 - F_c^2)^2]/\sum[w(F_o^2)^2]\}^{1/2}$.

Single-crystal X-ray diffraction: Single-crystal X-ray diffraction data for **1** was recorded on a Bruker Apex CCD II area-detector diffractometer with graphite-monochromated $Mo_{K\alpha}$ radiation (λ = 0.71073 Å) at 296(2) K. Absorption corrections were applied using multi-scan technique and performed by using the SADABS program[1]. The structures of **1** was solved by direct methods and refined on F^2 by full-matrix leastsquares methods by using the SHELXTL package[2]. The numbers of lattice water molecules and counter cations for **1** was estimated by the results of elemental analyses, TG curves, and calculations of electron count in the voids with SQUEEZE[3].

During the refinement, all the non-H atoms were refined anisotropically. In the crystal structure, no H atoms on these O atoms could be found from the difference Fourier map. All H atoms on solvent water molecules were included into the formula directly.

The highest residue peak 3.858 eA^3 and the deepest hole is -1.312 eA^3.

About 11.5 solvent water molecules, 9 Na^+ cations were found from the Fourier maps, however, there are still a very large accessible solvent voids in the crystal structure caculated by SQUEEZE subroutine of PLATON software, indicating that some more water molecules or cations should exist in the structure, but cannot be found from the weak residual electron peaks. Based on the TGA curve and elemental analyses, another 19 Na^+ cations and 19.5 H_2O were included into the molecular formula directly.

References:

[1] Sheldrick, G. *SADABS*; ver. 2.10; University of Gottingen: Göttingen, Germany, **2003**.

[2] A.L. Spek, *Acta Cryst.* (**2015**). C71, 9–18.

[3] Spek, A. L. *PLATON, A Multipurpose Crystallographic Tool*; Utrecht University, Utrecht, The Netherlands, **2003**.

1.3 Structure of 1

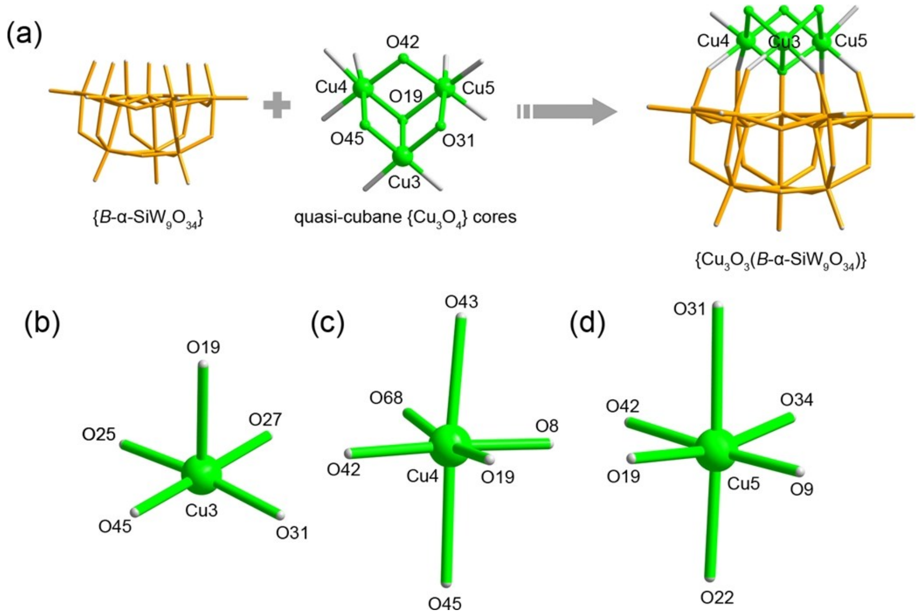

Fig. S1 Ball-and-stick representation of tri-copper-substituted Keggin-type {Cu_3SiW_9} subunit featuring a quasi-cubane {Cu_3O_4} core (a) and its coordination environment of Cu centers (b-d). Color code: Cu (green); W and Si (orange); and O (gray).

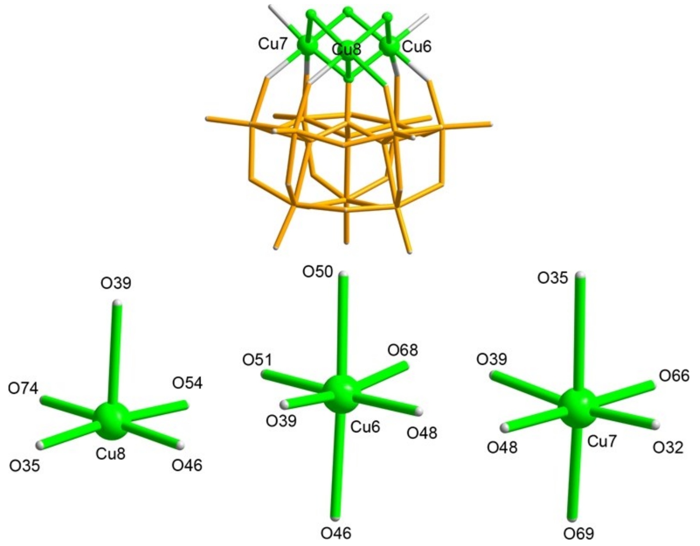

Fig. S2 Ball-and-stick representation of another {Cu_3SiW_9} subunit (top) and its coordination environment of Cu centers (down). Color code: Cu (green); W and Si (orange); and O (gray).

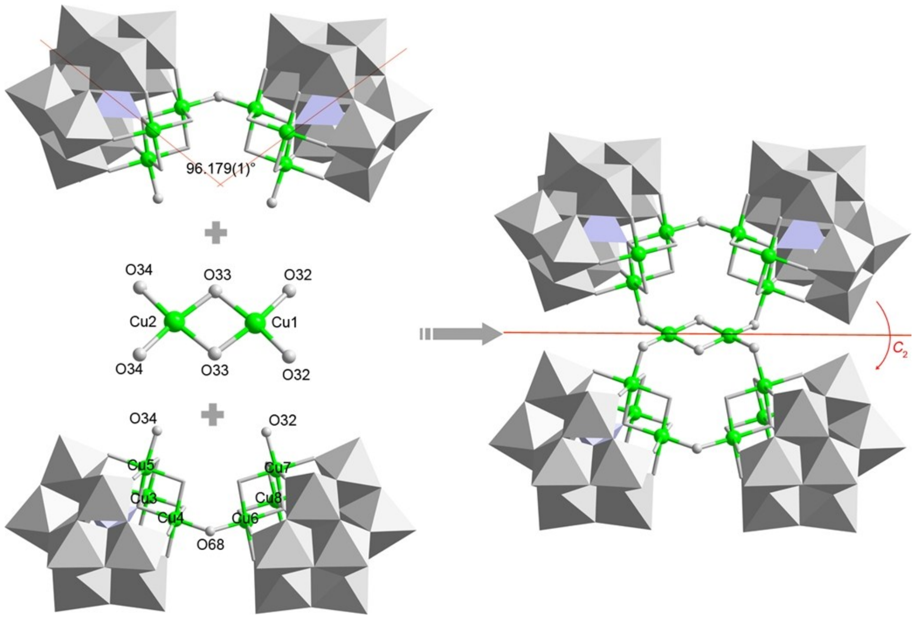

Fig. S3 Polyhedral and ball-and-stick representation of the formation of Cu_{14} cluster in **1a**. Color code: Cu (green); Si (cyan); and WO_6 (gray).

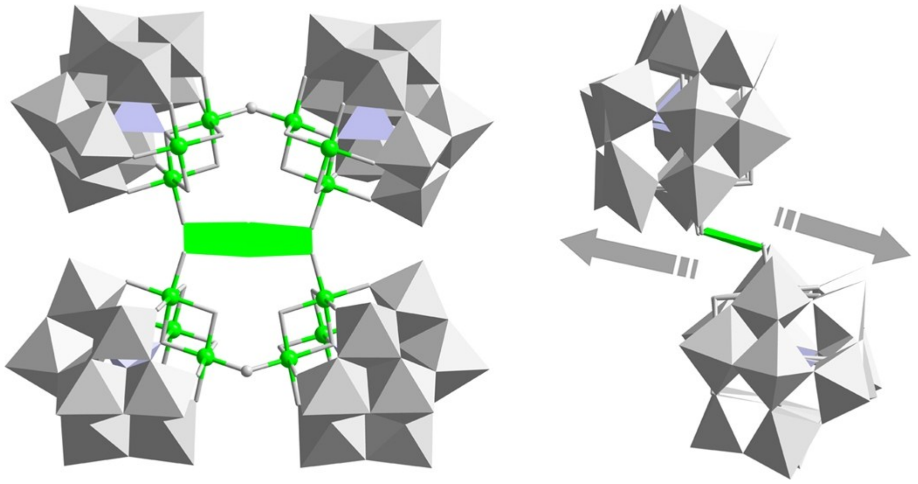

Fig. S4 Polyhedral and ball-and-stick representation of central $\{Cu_2O_6\}$ plane in **1a**. Color code: Cu (green); Si (cyan); and WO_6 (gray).

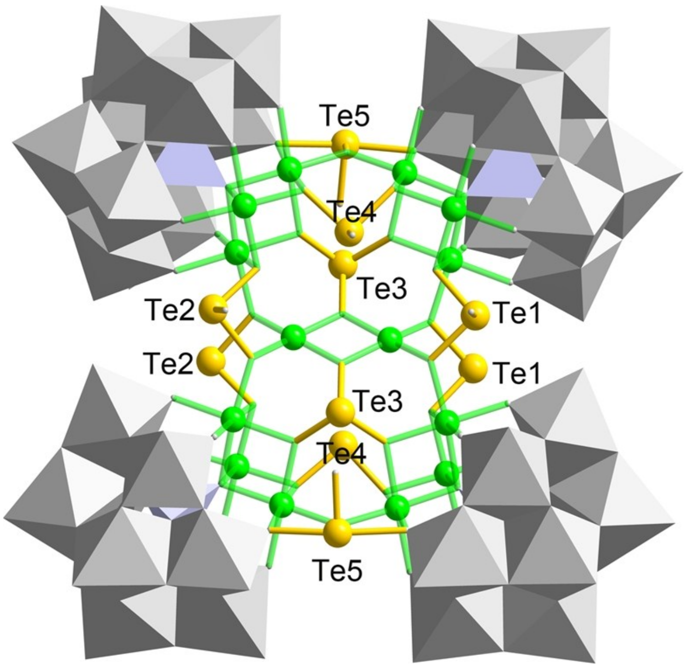

Fig. S5 Polyhedral and ball-and-stick representation of ten tellurite anions in **1a**. Color code: Cu (green); Te (yellow); Si (cyan); and WO_6 (gray).

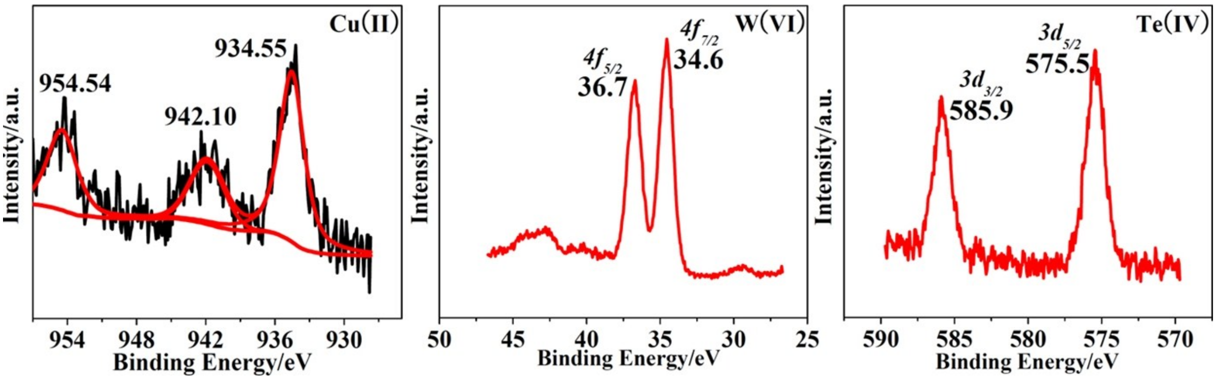

Fig. S6 W, Cu, and Te XPS spectra of **1**.

X-ray photoelectron spectroscopy (XPS) investigation was performed to confirm the valence states, indicating that the oxidation states of all W, Te, and Cu centers are +6, +4, and +2, respectively. The W element presents the peaks around 36.7 and 34.6 eV, which are in agreement with the energy regions of W $4f_{5/2}$ and W $4f_{7/2}$ ascribed to W^{6+} centers (*Cryst. Growth Des.*, 2001, **1**, 473). As for tellurium(IV), the Te $3d_{3/2}$ and Te $3d_{5/2}$ peaks are observed at 585.9 and 575.5 eV, respectively (*J. Phys. Chem. C*, 2011, **115**, 16524). The peaks around 934.55 eV, 942.10 eV and 954.54 eV in the energy regions of Cu $2p_{3/2}$ and Cu $2p_{1/2}$ correspond to Cu^{2+} (*Catal. Sci. Technol.*, 2015, **5**, 5174; *CrystEngComm*, 2016, **18**, 3650–3654).

Table S2. Bond Valence Sum (BVS) of all Cu atoms.

Atom	BVS value	Atom	BVS value
Cu1	1.874	Cu5	1.817
Cu2	1.847	Cu6	1.927
Cu3	1.973	Cu7	1.886
Cu4	1.904	Cu8	1.883

1.4 Selected Bond Lengths and Angles for the Cu and Te Atoms in 1

Table S3. Selected Cu-O bond lengths for **1**.

bond	d (Å)	bond	d (Å)	bond	d (Å)	bond	d (Å)
Cu(1)-O(33)$^{\#3}$	1.91(2)	Cu(3)-O(25)	1.92(2)	Cu(5)-O(9)	1.94(2)	Cu(7)-O(32)	1.95(2)
Cu(1)-O(33)	1.91(2)	Cu(3)-O(45)	1.92(2)	Cu(5)-O(34)$^{\#3}$	1.94(2)	Cu(7)-O(48)$^{\#3}$	1.96(2)
Cu(1)-O(32)	1.95(2)	Cu(3)-O(27)	1.95(2)	Cu(5)-O(42)	2.01(2)	Cu(7)-O(66)$^{\#3}$	1.96(2)
Cu(1)-O(32)$^{\#3}$	1.95(2)	Cu(3)-O(31)	1.95(2)	Cu(5)-O(19)	2.04(2)	Cu(7)-O(39)$^{\#3}$	2.01(2)
Cu(1)-Cu(2)	2.955(7)	Cu(3)-O(19)	2.42(2)	Cu(5)-O(22)	2.28(2)	Cu(7)-O(69)$^{\#3}$	2.24(3)
Cu(2)-O(33)	1.93(2)	Cu(4)-O(8)	1.94(2)	Cu(6)-O(68)	1.95(2)	Cu(8)-O(35)	1.92(2)
Cu(2)-O(33)$^{\#3}$	1.93(2)	Cu(4)-O(68)	1.95(2)	Cu(6)-O(39)	1.95(2)	Cu(8)-O(74)	1.95(3)
Cu(2)-O(34)$^{\#3}$	1.94(2)	Cu(4)-O(19)	1.97(2)	Cu(6)-O(51)	1.98(2)	Cu(8)-O(46)	1.95(2)
Cu(2)-O(34)	1.94(2)	Cu(4)-O(42)	1.98(2)	Cu(6)-O(48)	2.04(2)	Cu(8)-O(54)	1.99(2)
		Cu(4)-O(43)	2.29(2)	Cu(6)-O(50)	2.32(3)	Cu(8)-O(39)	2.44(3)
		Cu(4)-Cu(5)	2.968(5)	Cu(6)-O(46)	2.43(3)		
				Cu(6)-Cu(7)$^{\#3}$	2.980(5)		

$^{\#3}$ x+0,-y+1/2,-z+1/4

Table S4. Selected Te-O bond lengths and angles for **1**.

bond	d (Å)	angles	Degree (°)
Te(1)-O(36)	1.70(3)	O(36)-Te(1)-O(35)	98.7(12)
Te(1)-O(35)	1.88(2)	O(36)-Te(1)-O(32)	100.8(12)
Te(1)-O(32)	1.95(2)	O(35)-Te(1)-O(32)	89.3(9)
Te(2)-O(37)	1.86(2)	O(37)-Te(2)-O(31)	98.6(10)
Te(2)-O(31)	1.90(2)	O(37)-Te(2)-O(34)	98.2(10)
Te(2)-O(34)	1.94(2)	O(31)-Te(2)-O(34)	88.5(9)
Te(3)-O(48)	1.85(2)	O(48)-Te(3)-O(42)	96.2(9)
Te(3)-O(42)	1.87(2)	O(48)-Te(3)-O(33)	93.0(9)
Te(3)-O(33)	1.925(19)	O(42)-Te(3)-O(33)	93.1(9)
Te(3)-O(82)	2.46(2)	O(48)-Te(3)-O(82)	90.1(9)
Te(4)-O(45)	1.87(2)	O(42)-Te(3)-O(82)	86.1(8)
Te(4)-O(47)	1.88(2)	O(33)-Te(3)-O(82)	176.9(9)
Te(4)-O(46)	1.91(2)	O(45)-Te(4)-O(47)	97.7(10)
Te(5)-O(82)	1.84(2)	O(45)-Te(4)-O(46)	93.2(9)
Te(5)-O(68)	1.89(2)	O(47)-Te(4)-O(46)	96.3(11)
Te(5)-O(43)	2.10(2)	O(82)-Te(5)-O(68)	98.0(10)
Te(5)-O(50)	2.11(2)	O(82)-Te(5)-O(43)	88.5(9)
		O(68)-Te(5)-O(43)	80.5(9)
		O(82)-Te(5)-O(50)	91.5(9)
		O(68)-Te(5)-O(50)	82.7(10)
		O(43)-Te(5)-O(50)	163.1(9)

Section 2 Water Reducion Experimental Section

Elemental analyses of Cu, W and Na were performed on a PLASMA-SPEC (I) inductively coupled plasma (ICP) atomic emission spectrometer. Water contents were determined by TG analyses on a PerkinElmer TGA7 instrument in flowing N_2 with a heating rate of 10 °C min^{-1}. UV/Vis absorption spectra were obtained by using a 752 PC UV/Vis spectrophotometer. XRD studies were performed with a Rigaku D/max-IIB X-ray diffractometer at a scanning rate of 1° min^{-1} with $Cu_{K\alpha}$ radiation (λ = 1.5418 Å). IR spectra were recorded on an Alpha Centauri FTIR spectrophotometer on pressed KBr pellets in the range 400~4000 cm^{-1}. XPS was performed on a VG ESCALABMKII spectrometer with an $Mg_{K\alpha}$ (1253.6 eV) achromatic X-ray source. The vacuum inside the analysis chamber was maintained at 6.2×10^{-6} Pa during the analysis. DLS measurements were done by using a Zetasizer NanoZS (Malvern Instruments). Contact angles were measured on a KRÜSS DSA20MK2 Drop Shape Analysis System. The emission spectra were recorded using the F-7000 FL spectropho-tometer under 455 nm excitation.

Photocatalytic H_2 evolution Measurements. The H_2 evolution experiments were performed in a closed gas-circulating system equipped with an external illumination Pyrex reaction vessel (total volume 50 mL) with a magnetic stirrer for vigorous stirring (1.0×10^3 rpm) and analyzed by using an automatic H_2 monitoring system. The vessel was filled with a solution containing a photosensitizer $[Ir(ppy)_2(dtbbpy)][PF_6]$ (0.2 mM), a sacrificial electron donor TEOA (1 mL), CH_3CN (5.5 mL), DMF (16.5 mL), H_2O (2 mL) and different concentrations of catalysts **1** (0–20 μM). Then, photosensitizer $[Ir(ppy)_2(dtbbpy)][PF_6]$ (0.2 mM) was finally added quickly in last after putting all contents of reaction mixture and the system was evacuated in the dark to remove the air completely. The reaction was performed using a 100 W Xe lamp equipped with a long-pass filter (420 nm cut off). The produced H_2 was automatically (25 min^{-1}) analyzed by gas chromatography with a GC7890T instrument with a thermal conductivity detector (TCD) and a 5 Å molecular sieve column (2 m × 3 mm) using Ar as carrier gas.

Table S5. Visible light-driven H_2 evolution catalyzed by different concentrations of **1** and corresponding contrast experiments.

Entry	Catalysts	Catalyst concentration (μM)	Moles of H_2 evolved (μmol)	TON[b]	TOF[c] [h^{-1}]
1	**1**[a]	0	4.241	-	-
2	**1**	2	17.18	343.6	116.7
3	**1**	5	20.52	164.2	76.99
4	**1**	10	26.37	105.5	51.52
5	**1**	15	31.59	84.25	44.53
6	**1**	20	39.79	79.58	43.14
7	Cu^{2+}	70	8.664	4.951	2.170
8	Cu^{2+} and TeO_3^{2-}	70/50	8.856	-	-
9	Cu^{2+} and SiW_9	70/10	8.569	-	-
10	SiW_9	10	4.222	-	-
11	TeO_3^{2-}	50	4.234	-	-

[a] Conditions: 100 W Xe lamp equipped with a long-pass filter (420 nm cut off); catalysts **1** (0–20 μM) in a 25 mL solution (1 mL TEOA, 5.5 mL CH_3CN, 16.5 mL DMF, and 2 mL H_2O) with photosensitizer $[Ir(ppy)_2(dtbbpy)][PF_6]$ (0.2 mM) after 10 h of visible-light irradiation; vigorous stirring (1.0×10^3 rpm). [b] TON = mol of H_2/mol of catalyst. [c] $TOF_{initial}$ = mol of H_2/(mol of catalyst × 0.5 h), based on the amount of H_2 produced after 0.5 h of irradiation.

Table S6. Visible light-driven H_2 evolution catalyzed by different transition-metal-substituted POMs-based catalyst using Ru or Ir complex photosensitizer.

Transition-metal	Year	Catalysts	Representative reaction conditions	TON	TOF	Ref.
manganese	2013	$[Mn_4(H_2O)_2(VW_9O_{34})_2]^{10-}$	LED light (20 mW, 455 nm), 0.67 mM $[Ru(bpy)_3]Cl_2$, TEOA (0.25 M), 2 mL DMF/H_2O (1.86/1)	42	-	Ref. 1
	2016	$[MnMo_6O_{18}\{(OCH_2)_3CNCH\text{-}bpy\text{-}Ir(ppy)_2\}_2]^{1-}$ (Ir-photosensitized POM complex)	LED light (λ_{max}=470 nm) DMF (4.3 mL), TEA (1 M), AcOH (0.2 M), catalyst (0.1 mM)	80	-	Ref. 2
	2017	$[MnMo_6O_{18}\{(OCH_2)_3CNCH(IrC_{33}H_{26}N_4)\}_2]^{1-}$ (Ir-photosensitized POM complex)	LED light (λ_{max}=470 nm) DMF (4.3 mL), TEA (1 M), AcOH (0.2 M), catalyst (0.1 mM)	80	-	Ref. 3
nickel	2013	$[P_2W_{17}O_{61}\{O(SiC_{36}H_{23}N_3O_2Ir)_2\}]^{6-}$ (DSi[Ir]) (Ir-photosensitized POM complex)	300 W Xe (400 nm cut off), DMF (10 mL), NEt_3 (1 M) AcOH (0.1 M), DSi[Ir] (0.2 mM).	41	-	Ref. 4
	2014	$[Ni_4(H_2O)_2(PW_9O_{34})_2]^{10-}$	LED light (20 mW, 455 nm), $[Ir(ppy)_2(dtbbpy)]^+$ (0.2 mM), TEOA (0.25 M), H_2O (1.4 M), 4 mL CH_3CN/DMF (1/3)	6500	-	Ref. 5
	2015	$[\{Ni_4(OH)_3AsO_4\}_4(B\text{-}\alpha\text{-}PW_9O_{34})_4]^{28-}$	LED light (20 mW, 455 nm), 0.2 mM $[Ir(ppy)_2(dtbbpy)][PF_6]$, TEOA (0.25 M), H_2O (1.4 M), CH_3CN/DMF (1:3 v/v, 2 mL)	580	-	Ref. 6
	2015	$[Ni(H_2O)PW_{11}O_{39}]^{5-}$ $[Ni(H_2O)SiW_{11}O_{39}]^{6-}$ $[Ni(H_2O)GeW_{11}O_{39}]^{6-}$	High power LED (λ = 470 nm), 1.0 mM $[Ru(bpy)_3]Cl_2$, 0.12 M ascorbate buffer, pH 4	10.8 inactive 36.8	0.0097 s^{-1} - 0.009 s^{-1}	Ref. 7
	2016	$[Ni_3(OH)_3(H_2O)_3P_2W_{15}O_{59}]^{9-}$	LED light (20 mW, 455 nm), 0.2 mM $[Ir(ppy)_2(dtbbpy)][PF_6]$, TEOA (0.25 M), CH_3CN/DMF (1:3 v/v, 2 mL)	160	-	Ref. 8
	2017	$[\{Ni_4(OH)_3(PO_4)\}_4(A\text{-}PW_9O_{34})_4]^{28-}$	100 W LED light (400–	578.8	100.5 h^{-1}	Ref. 9

		$[\{Ni_4(OH)_3(PO_4)\}_4(A\text{-}PW_9O_{34})_2(B\text{-}PW_9O_{34})_2]^{28-}$ $[\{Ni_4(OH)_3(VO_4)\}_4(B\text{-}PW_9O_{34})_4]^{28-}$	780 nm), 0.2 mM $[Ir(ppy)_2(dtbbpy)][PF_6]$, 2 mL TEOA, 11 mL CH_3CN, 33 mL DMF, and 4 mL H_2O	679.1 931.1	112.7 h^{-1} 185.5 h^{-1}	
copper	2016	$[Cu_4(H_2O)_2(B\text{-}\alpha\text{-}PW_9O_{34})_2]^{10-}$ (dominant active species)	LED light (20 mW, 455 nm), $[Ir(ppy)_2(dtbbpy)]^+$ (0.2 mM), TEOA (0.25 M), H_2O (1.4 M), 2 mL CH_3CN/DMF (1/3)	1270	-	Ref. 10
	2018	$[Cu^{II}_{14}Te^{IV}_{10}O_{28}(B\text{-}\alpha\text{-}SiW_9O_{34})_4]^{28-}$	Xe light (100 W, 420 nm cut off), 0.2 mM $[Ir(ppy)_2(dtbbpy)][PF_6]$, 1 mL TEOA, 5.5 mL CH_3CN, 16.5 mL DMF, and 2 mL H_2O	343.6	116.7 h^{-1}	this work

References:

(1) H. Lv, J. Song, H. Zhu, Y. V. Geletii, J. Bacsa, C. Zhao, T. Lian, D. G. Musaev and C. L. Hill, *J. Catal.* 2013, **307**, 48–54.

(2) S. Schönweiz, S. A. Rommel, J. Kübel, M. Micheel, B. Dietzek, S. Rau and C. Streb, *Chem. Eur. J.*, 2016, **22**, 12002–12005.

(3) S. Schönweiz, M. Heiland, M. Anjass, T. Jacob, S. Rau and C. Streb, *Chem. Eur. J.*, 2017, **23**, 15370–15376.

(4) B. Matt, J. Fize, J. Moussa, H. Amouri, A. Pereira, V. Artero, G. Izzet and A. Prousta, *Energy Environ. Sci.*, 2013, **6**, 1504–1508.

(5) H. Lv, W. W. Guo, K. Wu, Z. Chen, J. Bacsa, D. G. Musaev, Y. V. Geletii, S. M. Lauinger, T. Lian and C. L. Hill, *J. Am. Chem. Soc.*, 2014, **136**, 14015–14018.

(6) H. Lv, Y. Chi, J. V. Leusen, P. Kögerler, Z. Chen, J. Bacsa, Y. V. Geletti, W. Guo, T. Lian, and C. L. Hill, *Chem. Eur. J.*, 2015, **21**, 17363–17370.

(7) K. von Allmen, R. Moré, R. Müller, J. Soriano-López, A. Linden and G. R. Patzke, *ChemPlusChem*, 2015, **80**, 1389–1398.

(8) W. Guo, H. Lv, J. Bacsa, Y. Gao, J. S. Lee and C. L. Hill, *Inorg. Chem.*, 2016, **55**, 461−466.

(9) X.-B. Han, C. Qin, X.-L. Wang, Y.-Z. Tan, X.-J. Zhao and E.-B. Wang, *Appl. Catal., B* 2017, **211**, 349–356.

(10) H. Lv, Y. Gao, W. Guo, S. M. Lauinger, Y. Chi, J. Bacsa, K. P. Sullivan, M. Wieliczko, D. G. Musaev and C. L. Hill, *Inorg. Chem.*, 2016, **55**, 6750–6758.

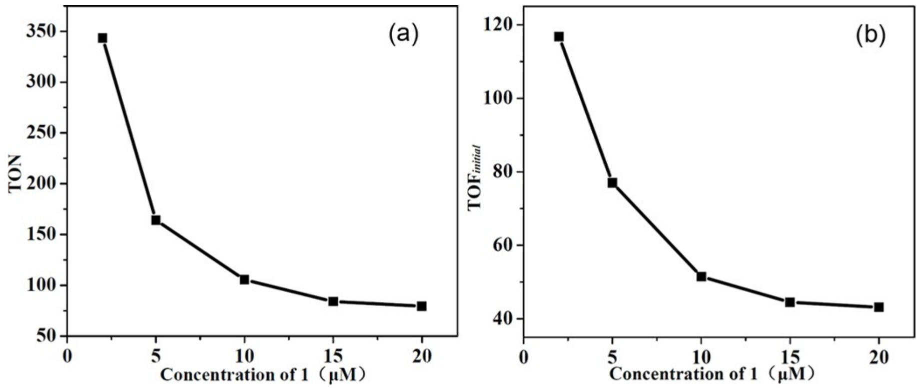

Fig. S7 TON *vs.* or TOF$_{initial}$ catalyst concentration for **1**.

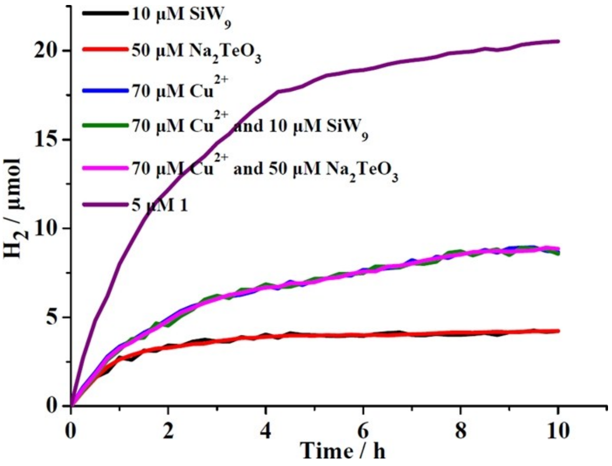

Fig. S8 Kinetics of H_2 evolution of the photocatalytic system with **1**, $CuCl_2$, SiW_9, and Na_2TeO_3. Conditions: 100 W Xe lamp equipped with a long-pass filter (420 nm cut off); 25 mL solution (1 mL TEOA, 5.5 mL CH_3CN, 16.5 mL DMF, and 2 mL H_2O) with photosensitizer [Ir(ppy)$_2$(dtbbpy)][PF$_6$] (0.2 mM) after 10 h of visible-light irradiation; vigorous stirring (1.0×10^3 rpm).

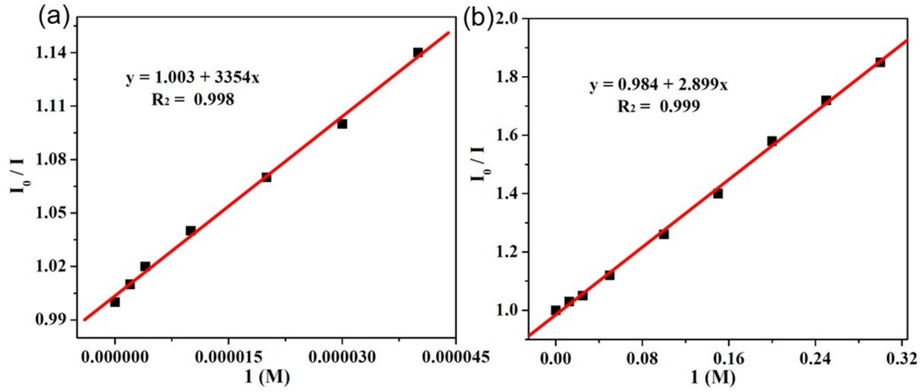

Fig. S9 Stern-Volmer plots for emission spectra of [Ir(ppy)$_2$(dtbbpy)]$^+$ as a function of added (a) **1**, and (b) TEOA.

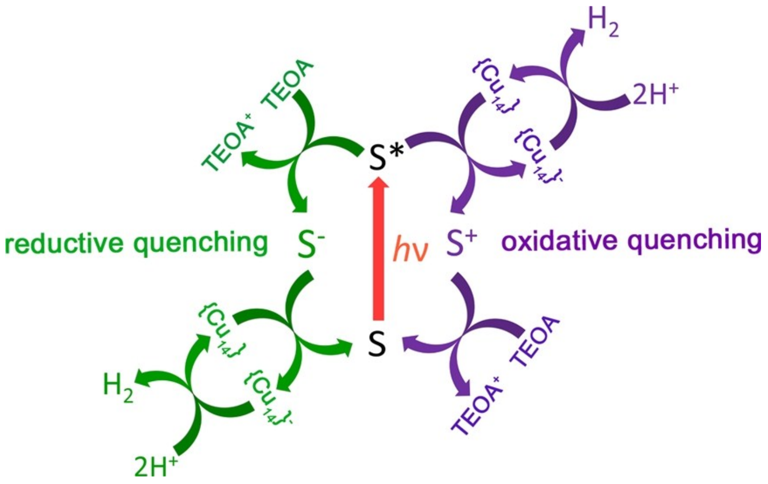

Scheme S1. Proposed mechanism for the homogeneous H_2 evolution system catalyzed by **1** with oxidative quenching and reductive quenching mechanism.

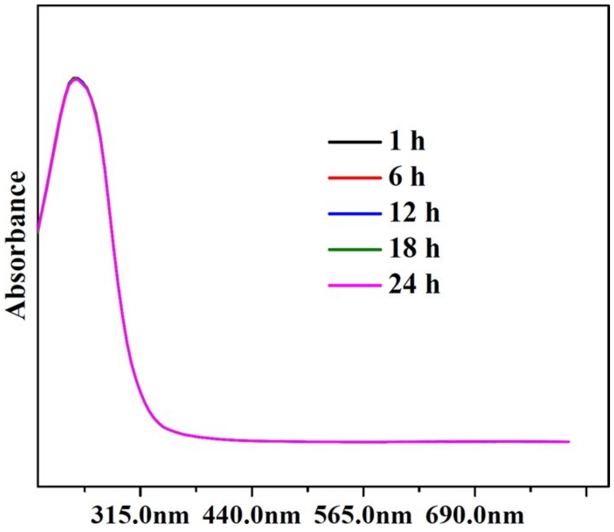

Fig. S10 Time-dependent UV-Vis spectrum of **1** under nonturnover conditions. The UV-Vis curves remained almost unchanged with time.

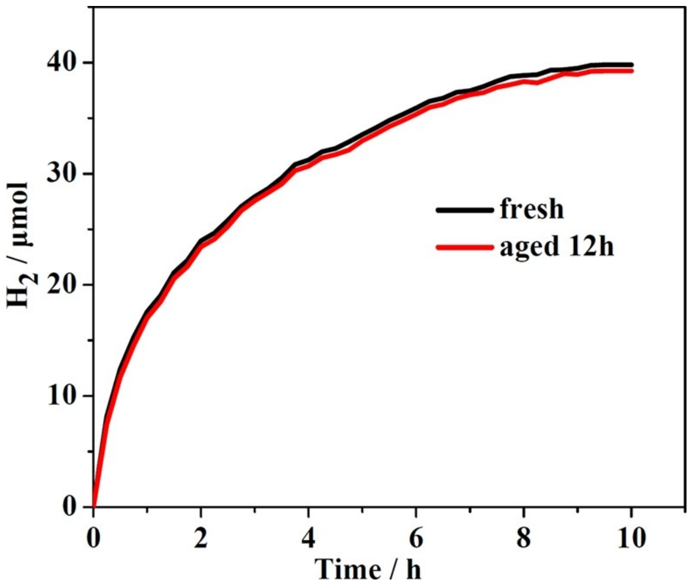

Fig. S11 The photocatalytic H_2 evolution activities of **1** after being aged for 12h were similar to that of the fresh catalyst.

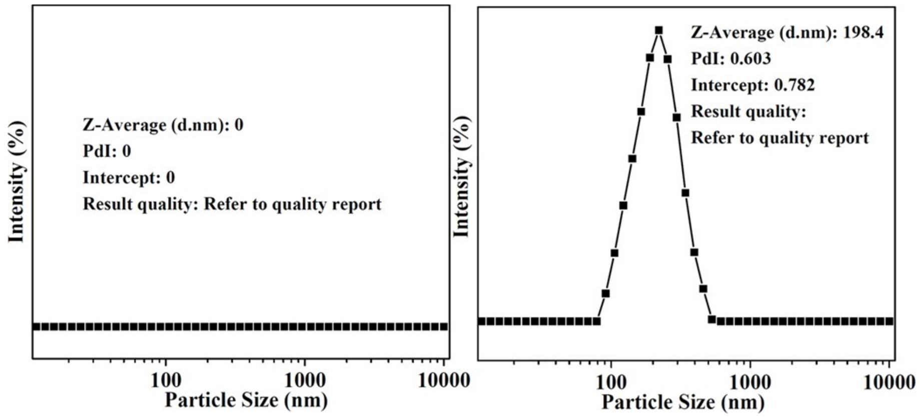

Fig. S12 DLS measurement of a photocatalytic H_2 evolution solution of **1** (left) or $CuCl_2$ (25 μM) (right) after 10 h of visible-light irradiation. No nanoparticles is detected by DLS in **1**-catalyzed post-reaction solution, while nanoparticles with diameters intensively distributed around 198.4 nm are formed after $CuCl_2$-catalyzed reactions observed by DLS (Fig. S12). This result indicated that **1** itself did serve as true molecular catalysts and did not decompose into Cu^{2+}(aq), copper hydroxide or/and copper oxide nanoparticles under the irradiation/catalytic conditions.

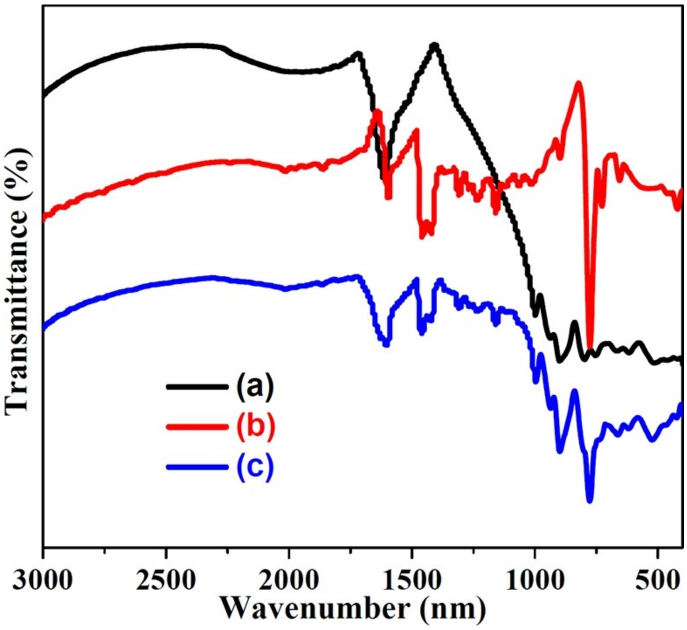

Fig. S13 Solid-state FT-IR spectra of pristine **1** (a), $[Ru(bpy)_3]Cl_2$ (b), $[Ru(bpy)_3]^{2+}$ salt of **1** (c) isolated after light-driven reaction (isolated from post-catalytic reaction solution). **1** was isolated from post-reaction solution treated with excess $[Ru(bpy)_3]^{2+}$ for FT-IR spectra analysis, which remains no changes compared to the spectrum before catalytic reaction (Fig. S13). This result indicates the framework of **1** remains intact before and after the light-driven reactions.

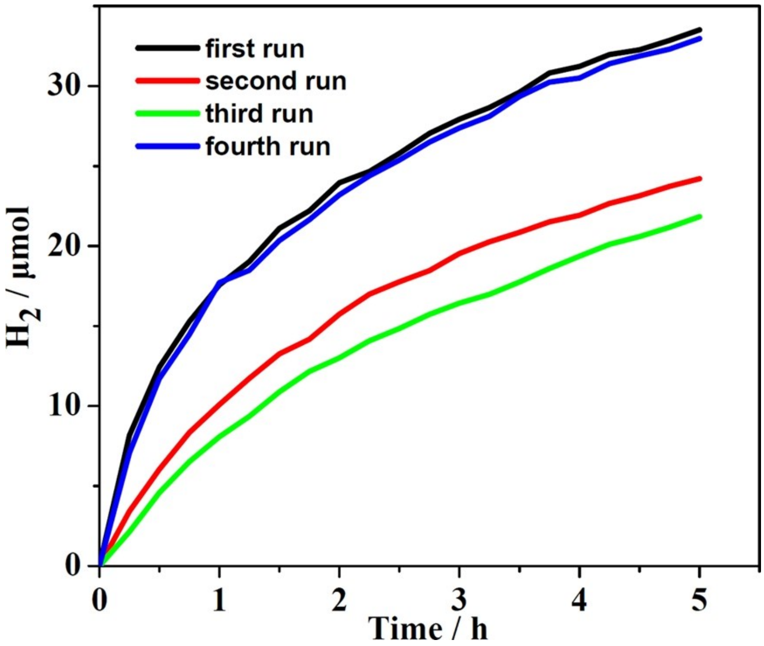

Fig. S14 Visible light-driven H_2 formation kinetics of the first run (black line), the second run (red line), the third run (green line), and the fourth run (blue line) of **1**.

The reusability experiment of **1** was carried out for further exploring the stability under the irradiation/catalytic conditions. As shown in Fig. S14, the yield of H_2 generation decreases in three successive runs with **1**-containing reactions. After every 5 h of irradiation, the H_2 evolution amounts for the first, second, and third run are 32.9 µmol, 24.2 µmol, and 21.8 µmol, respectively. This can be attributed to a slight degradation of the $[Ir(ppy)_2(dtbbpy)][PF_6]$ light absorber and consumption of TEOA. To prove this hypothesis, 0.4 ml H_2O, 0.1 ml TEOA, and 1.8×10^{-3} µmol $[Ir(ppy)_2(dtbbpy)][PF_6]$ were added to the photocatalytic system after the third run. The H_2 evolution amount is similar as the first run after 5 h of irradiation (Fig. S14, blue line).

We also performed other reusability experiments of **1**. After the first run, 0.4 mL H_2O was added to the photocatalytic system for the second run. After 5 h of irradiation, the H_2 evolution amount was comparable to the red line of Fig. S14. Then, 0.1 ml TEOA was added to the reaction system for the third run. After 5 h of irradiation, the H_2 evolution amount was almost no change compared to the green line of Fig. S14. Finally, 1.8×10^{-3} µmol $[Ir(ppy)_2(dtbbpy)][PF_6]$ was added to the photocatalytic reaction system after the third run. After 5 h of irradiation, the H_2 evolution amount was also comparable to the blue line of Fig. S14. In addition, 1.8×10^{-3} µmol$[Ir(ppy)_2(dtbbpy)][PF_6]$ was added to the photocatalytic reaction system after the first run and the H_2 evolution amount was similar as the first run after 5 h of irradiation. These results indicated $[Ir(ppy)_2(dtbbpy)][PF_6]$ might be a dominant factor that influence the H_2 evolution activities.

Section 3 Supplementary Physical Characterizations

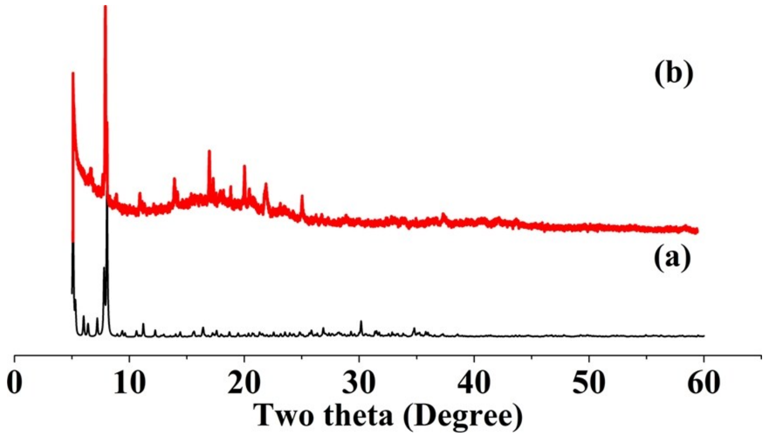

Fig. S15 The XRPD patterns for as-synthesized (b) and simulated (a)

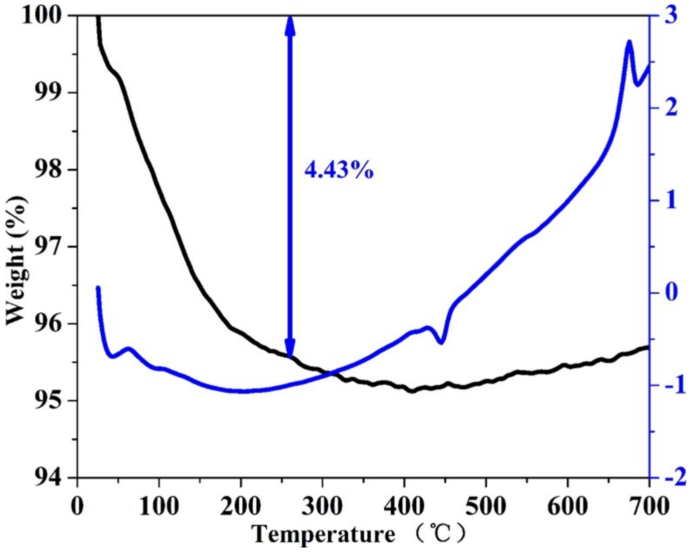

Fig. S16 TG-DTA curve of **1**. (The main weight loss is corresponding to the loss of lattice water molecules (from 25 to ca. 250 °C) and then the structure begans to decompose.)